Electro-optic light modulation and THz generation in locally plasma-activated silicon nanophotonic devices

Christopher Matheisen,[1,2,*] Michael Waldow,[2] Bartos Chmielak,[1] Simon Sawallich,[1] Thorsten Wahlbrink,[2] Jens Bolten,[2] Michael Nagel[2] and Heinrich Kurz[1,2]

[1]*Institute of Semiconductor Electronics (IHT), RWTH Aachen University, Sommerfeldstraße 24, 52074 Aachen, Germany*

[2]*AMO GmbH, Otto-Blumenthal-Straße 25, 52074 Aachen, Germany*

**matheisen@amo.de*

Abstract: Silicon is not an electro-optic material by itself but the required second-order optical nonlinearity can be induced by breaking the inversion symmetry of the crystal lattice. Recently, an attractive approach has been demonstrated based on a surface-activation in a CMOS-compatible HBr dry etching process. In this work, we further investigate and quantify the second-order nonlinearity induced by this process. Using THz near-field probing we demonstrate that this simple and versatile process can be applied to locally equip silicon nanophotonic chips with micro-scale areas of electro-optic activity. The realization of a first fully integrated Mach-Zehnder modulator device – based on this process – is applied to quantify the nonlinearity to an effective $\chi^{(2)}$ of 9 ± 1 pm/V. Analysis of the thermal stability of the induced nonlinearity reveals post-processing limitations and paths for further efficiency improvements.

OCIS codes: (130.0130) Integrated optics; (250.7360) Waveguide modulators; (190.0190) Nonlinear optics; (160.2100) Electro-optical materials; (190.4223) Nonlinear wave mixing; (110.6795) Terahertz imaging.

References and links

1. G. Reed, G. Mashanovich, F. Gardes, and D. Thomson, "Silicon optical modulators," Nat. Photonics **4**(8), 518–526 (2010).
2. C. Schriever, C. Bohley, J. Schilling, and R. B. Wehrspohn, "Strained silicon photonics," Materials **5**(12), 889–908 (2012).
3. R. S. Jacobsen, K. N. Andersen, P. I. Borel, J. Fage-Pedersen, L. H. Frandsen, O. Hansen, M. Kristensen, A. V. Lavrinenko, G. Moulin, H. Ou, C. Peucheret, B. Zsigri, and A. Bjarklev, "Strained silicon as a new electro-optic material," Nature **441**(7090), 199–202 (2006).
4. J. Fage-Pedersen, L. H. Frandsen, A. V. Lavrinenko, and P. I. Borel, "A linear electro-optic effect in silicon, induced by use of strain," in *3rd IEEE International Conference on Group IV Photonics*, 37–39 (2006).
5. C. Koos, P. Vorreau, T. Vallaitis, P. Dumon, W. Bogaerts, R. Baets, B. Esembeson, I. Biaggio, T. Michinobu, F. Diederich, W. Freude, and J. Leuthold, "All-optical high-speed signal processing with silicon-organic hybrid slot waveguides," Nat. Photonics **3**(4), 216–219 (2009).
6. T. Baehr-Jones, M. Hochberg, R. Soref, and A. Scherer, "Design of a tunable, room temperature, continuous-wave terahertz source and detector using silicon waveguides," J. Opt. Soc. Am. B **25**(2), 261–268 (2008).
7. M. Gould, T. Baehr-Jones, R. Ding, S. Huang, J. Luo, A. K.-Y. Jen, J.-M. Fedeli, M. Fournier, and M. Hochberg, "Silicon-polymer hybrid slot waveguide ring-resonator modulator," Opt. Express **19**(5), 3952–3961 (2011).
8. R. Palmer, L. Alloatti, D. Korn, P. C. Schindler, R. Schmogrow, M. Baier, S. Koenig, D. Hillerkuss, J. Bolten, T. Wahlbrink, M. Waldow, R. Dinu, W. Freude, C. Koos, and J. Leuthold, "Silicon-Organic Hybrid (SOH) Modulator Generating up to 84 Gbit/s BPSK and *M*-ASK Signals," in *Optical Fiber Communication Conference*, Novel Modulators (Optical Society of America, 2013), paper OW4J.6.
9. S. Abel, T. Stöferle, C. Marchiori, C. Rossel, M. D. Rossell, R. Erni, D. Caimi, M. Sousa, A. Chelnokov, B. J. Offrein, and J. Fompeyrine, "A strong electro-optically active lead-free ferroelectric integrated on silicon," Nat Commun **4**, 1671 (2013).

#203363 - $15.00 USD Received 18 Dec 2013; revised 13 Feb 2014; accepted 17 Feb 2014; published 27 Feb 2014

10. M. Cazzanelli, F. Bianco, E. Borga, G. Pucker, M. Ghulinyan, E. Degoli, E. Luppi, V. Véniard, S. Ossicini, D. Modotto, S. Wabnitz, R. Pierobon, and L. Pavesi, "Second-harmonic generation in silicon waveguides strained by silicon nitride," Nat. Mater. **11**(2), 148–154 (2011).
11. B. Chmielak, M. Waldow, C. Matheisen, C. Ripperda, J. Bolten, T. Wahlbrink, M. Nagel, F. Merget, and H. Kurz, "Pockels effect based fully integrated, strained silicon electro-optic modulator," Opt. Express **19**(18), 17212–17219 (2011).
12. B. Chmielak, C. Matheisen, C. Ripperda, J. Bolten, T. Wahlbrink, M. Waldow, and H. Kurz, "Investigation of local strain distribution and linear electro-optic effect in strained silicon waveguides," Opt. Express **21**(21), 25324–25332 (2013).
13. M. Wächter, C. Matheisen, M. Waldow, T. Wahlbrink, J. Bolten, M. Nagel, and H. Kurz, "Optical generation of terahertz and second-harmonic light in plasma-activated silicon nanophotonic structures," Appl. Phys. Lett. **97**(16), 161107 (2010).
14. T. Wahlbrink, T. Mollenhauer, Y. M. Georgieva, W. Henschel, J. Efavi, H. Gottlob, M. Lemme, H. Kurz, J. Niehusmann, and P. Haring Bolivar, "Highly selective etch process for silicon-on-insulator nano-devices," Microel. Eng. **78–79**, 212–217 (2005).
15. M. Wächter, M. Nagel, and H. Kurz, "Tapered photoconductive terahertz field probe tip with subwavelength spatial resolution," Appl. Phys. Lett. **95**(4), 041112 (2009).
16. Y. J. Ding, "Quasi-single-cycle terahertz pulses based on broadband-phase-matched difference-frequency generation in second-order nonlinear medium: High output powers and conversion efficiencies," IEEE J. Sel. Top. Quantum Electron. **10**(5), 1171–1179 (2004).
17. N. K. Hon, K. K. Tsia, D. R. Solli, and B. Jalali, "Periodically poled silicon," Appl. Phys. Lett. **94**(9), 091116 (2009).
18. M. C. Flowers, N. B. H. Jonathan, Y. Liu, and A. Morris, "Temperature programmed desorption from the Si(100): Br and Si(100): D/Br surfaces: theory and experiment," Surf. Sci. **343**(1-2), 133–147 (1995).
19. R. B. Jackman, R. J. Price, and J. S. Foord, "Semiconductor surface etching by halogens: Fundamental steps," Appl. Surf. Sci. **36**(1-4), 296–312 (1989).
20. T. Shirao, K. Shudo, Y. Tanaka, T. Nakajima, T. Ishikawa, and M. Tanaka, "Thermal desorption process of bromide on Si(111) studied by highly sensitive mass spectroscopy," Jpn. J. Appl. Phys. **42**(Part 1, No. 2A), 593–596 (2003).
21. W. Kern and D. Puotinen, "Cleaning solutions based on hydrogen peroxide for use in silicon semiconductor technology," RCA Rev. **31**, 187 (1970).
22. H. Aizawa, S. Tsuneyuki, and T. Ogitsu, "Population analysis study of etching processes at Si(100) surfaces with adsorbed halogens and hydrogens," Surf. Sci. **438**(1-3), 18–25 (1999).
23. Q. Lin, O. J. Painter, and G. P. Agrawal, "Nonlinear optical phenomena in silicon waveguides: Modeling and applications," Opt. Express **15**(25), 16604–16644 (2007).
24. J. T. Robinson, K. Preston, O. Painter, and M. Lipson, "First-principle derivation of gain in high-index-contrast waveguides," Opt. Express **16**(21), 16659–16669 (2008).
25. A. Aleali, D. Xu, J. H. Schmid, P. Cheben, and W. N. Ye, "Optimization of stress-induced pockels effect in silicon waveguides for optical modulators," in 10*th* *IEEE International Conference on Group IV Photonics*, 109–110 (2013).
26. W. Luo, W. Guo, F. Xu, and Y.-Q. Lu, "Efficient surface second-harmonic generation in slot micro/nano-fibers," Opt. Express **21**(9), 11554–11561 (2013).

1. Introduction

Driven by the ongoing demand for higher bandwidth and cost reduction silicon photonics has seen a rapid development in recent years as an important platform for CMOS-compatible integrated optical devices [1,2]. However, the absence of second-order nonlinearity in pristine silicon is still hindering the fabrication of high-speed electro-optic modulators. Since silicon has a centrosymmetric crystal structure, second-order nonlinearities are forbidden in the dipole approximation. Recently, several approaches have been developed to endow silicon waveguides with second-order nonlinearity [2–13]. This is not only important for modulation applications but also for other nonlinear optical processes like difference frequency generation as e.g. used for all-optical terahertz signal generation [6,13].

A known method is to cover the silicon nanophotonic waveguide with a cladding layer of nonlinear active material. The evanescent field of a propagating guided mode in such a structure interacts with the nonlinear active cladding and generates an effective second-order nonlinearity [5–9]. Alternative to such hybrid approaches another basically different solution is to break the centrosymmetry of the silicon lattice itself by strain [10–12]. A first demonstration of a Pockels effect modulator based on globally strained silicon was published by Jacobsen et al. in 2006 [3]. A record value of strain-induced nonlinearity $\chi^{(2)}$ of 190 pm/V

#203363 - $15.00 USD Received 18 Dec 2013; revised 13 Feb 2014; accepted 17 Feb 2014; published 27 Feb 2014

has been achieved recently by Chmielak et al. by directly attaching silicon nitride straining layers on small cross-section silicon rib-waveguides [11,12].

Although these results are very promising still an unanswered question is how to implement these solutions into CMOS-compatible process lines and how to limit an induced electro-optic activity to dedicated chip areas. Recently, we have shown that a very simple CMOS-compatible process based on an HBr plasma-mediated chemical surface treatment, in the following denoted as plasma-activation (PA) is a promising alternative to induce second-order nonlinearity in silicon nanophotonic waveguides [13].

In this article we further investigate and highlight the specific advantages of the PA process in terms of its local applicability to generate spatially limited areas of nonlinear activity in waveguide sections of integrated photonic devices. The enhanced design capabilities are demonstrated by using novel THz near-field probes to directly visualize the micro-areas of electro-optic activity. Based on thermal stability measurement data a fabrication process for an integrated electro-optic modulator using PA is developed and realized into a first fully functional device. The modulator is based on an asymmetric Mach-Zehnder interferometer and utilized for the quantification of the achieved effective second-order nonlinearity.

2. Fabrication and inspection of locally plasma-activated waveguides

Locally plasma-activated silicon waveguides are fabricated from commercially available silicon-on-insulator (SOI) material with a phosphorous background doping of the silicon top layer and handle wafer resulting in a specific resistivity of < 22 Ωcm. The waveguides are structured and plasma-activated as described in [14] with a silicon top layer thickness of 220 nm and a waveguide width of 50 µm. Additional locally selective activation is realized by covering the surface with an E-Beam patterned PMMA masking layer before plasma activation. After the PA step, the PMMA masking layer is removed. The sample waveguide structure is intersected with a periodic pattern of plasma-activated rectangular areas as depicted in Fig. 1(a).

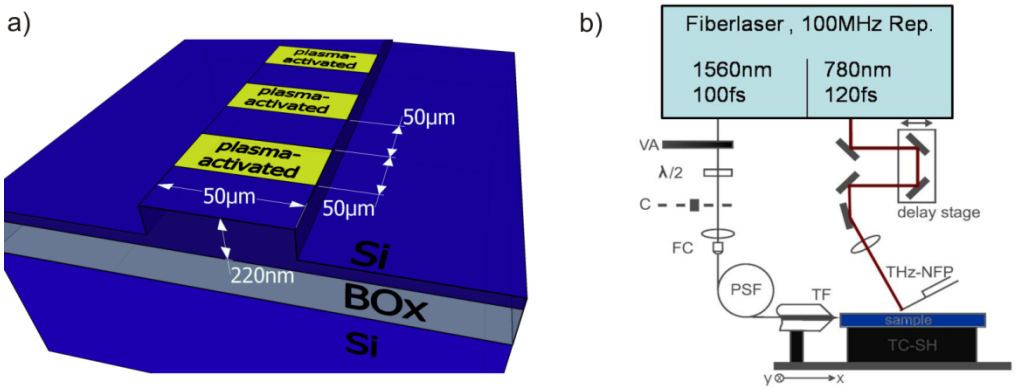

Fig. 1. (a) Periodically activated sample based on SOI with a 220 nm high and 50 µm wide rib waveguide. Yellow areas are exclusively exposed to the plasma-activation. (b) Schematic of the THz near-field setup (VA: variable attenuator, C: chopper, FC: fiber coupler, PSF: polarization maintaining singlemode fiber TF: tapered fiber tip, NFP: near-field probe, TC-SH: temperature controlled sample holder).

It has been shown earlier [13] that the induced second-order nonlinearity of the silicon waveguide can be utilized for the all-optical THz generation based on difference frequency generation (DFG). Using adequate near-field THz probe-tips [15] spatial investigations of the nonlinearity can be done by monitoring the local efficiency of THz light generation. The measurement set-up is based on a classic pump/probe scheme and sketched in Fig. 1(b). For optical excitation a femtosecond fiber laser system is applied which generates pulses of 100 fs

#203363 - $15.00 USD Received 18 Dec 2013; revised 13 Feb 2014; accepted 17 Feb 2014; published 27 Feb 2014

duration at 100 MHz repetition rate. The center-wavelength is 1560 nm. The pump beam is coupled via a polarization maintaining lensed fiber into the silicon waveguide with an average power of 5 mW at the fiber output.

As probing signal a frequency-doubled beam from the same laser-oscillator is focused on the photo-conductive gap of the freely positionable near-field probe tip. A motorized delay stage is used to adjust the time delay of the probe pulse. The set-up allows spatially and temporally resolved measurements of the THz near-field emission from the sample. By acquisition of field distributions in the near-field a sub-wavelength (λ/100) resolution has been obtained. The THz emission field strength is linear proportional to the effective $\chi^{(2)}$ coefficient [16]. Hence an image of the nonlinear activity is directly obtained. This technique has also been successfully applied for the local correlation of strain-gradients and second-order nonlinearity in silicon waveguides [11].

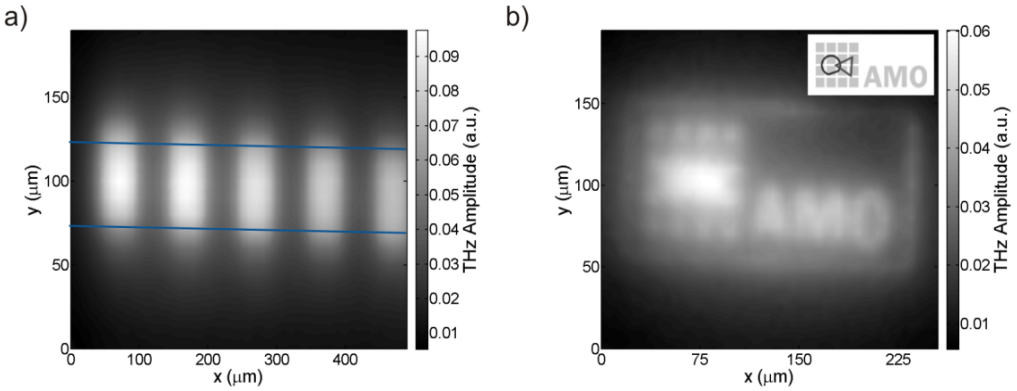

Fig. 2. Spatially resolved THz near-field measurement of locally plasma-activated silicon waveguides. (a) Periodically activated waveguide (Media 1) and (b) a logo patterned sample (inset shows the original logo).

Figure 2(a) shows the spatially resolved magnitude of the THz amplitude of the periodically activated waveguide accumulated over multiple measurements in a time interval of 1 ps. One can clearly identify the 50 µm long active areas followed by 50 µm inactive regions. The waveguide itself is lined out by blue lines in the image. Such a periodic structure could principally be applied for quasi-phase matched nonlinear frequency conversion as proposed by Hon et al. [17]. To further illustrate the design capabilities of our technique a "THz fluorescent writing" featuring the company logo of AMO GmbH (see inset of Fig. 2(b)) has been processed on a 100 µm wide silicon waveguide. Figure 2(b) again shows the spatially resolved THz near-field amplitude accumulated over 4 ps of time. The logo can be clearly recognized in the measurement although the smallest visible feature sizes in the measurement (given by the quadrates with 12 µm edge length and 7 µm spacing) are approximately two orders of magnitude smaller than the wavelength (300 µm to 3 mm) generated.

3. Thermal stability of the nonlinear optic activity

The temperature stability of the plasma-activated silicon surface is essential for the determination of any further required processing steps and can also give detailed information about the silicon-bromine surface bond species and their actual contribution to the nonlinear optical activity. A stepwise desorption of $SiBr_x$ surface bonds for increasing temperatures has been observed in earlier studies [18–20]. In contrast to common thermal desorption measurements, where steep thermal ramps are used to measure the thermally desorbed $SiBr_x$ molecules, we address here the degradation of nonlinear activity directly.

#203363 - $15.00 USD Received 18 Dec 2013; revised 13 Feb 2014; accepted 17 Feb 2014; published 27 Feb 2014

To provide a reliable starting point for the thermal annealing, a single plasma activated sample with 220 nm top silicon thickness without lateral structuring is diced into several pieces. For every temperature-dependent data point another piece is heated up to its specific target temperature. To prevent oxidation this step is done under nitrogen atmosphere. To ensure equilibrium state for each sample every target temperature is kept for one hour before smooth cool down. A reference sample was prepared for comparison using a standard cleaning procedure (RCA) [21]. After thermal annealing the THz emission amplitudes are measured for each sample under constant conditions using the same setup as introduced above.

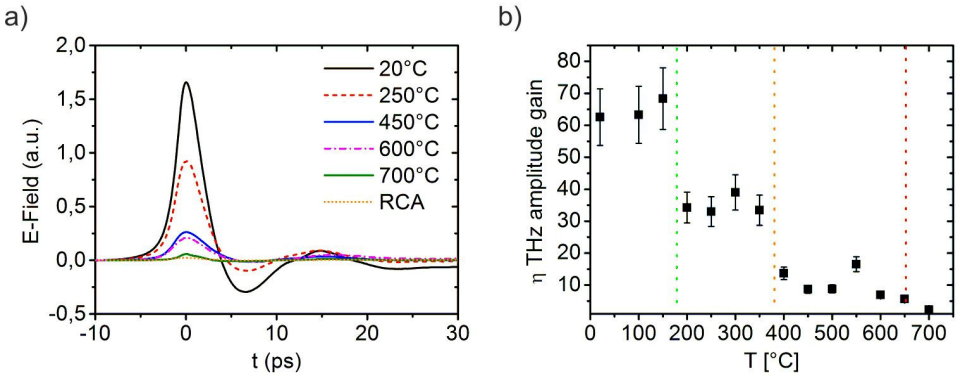

Fig. 3. THz emission of the differently annealed samples. (a) Time-domain THz field amplitude transients for different temperatures and a RCA cleaned sample. (b) THz amplitude gain factor referenced to a cleaned sample plotted against annealing temperature.

In Fig. 3(a) measured time-domain THz field transients are shown, taken at some exemplary annealing temperatures. The sample annealed at 250 °C exhibits a clear decrease of field amplitude in comparison to the 20 °C reference sample. The pulse shapes of these two samples are nearly unchanged.

At higher annealing temperatures the pulse amplitudes are further reduced and the pulse shapes are changing too. Especially the negative part of the signal is vanishing and converging to the signal shape of the RCA cleaned sample. This change in signal shape might be explained by the gradual removal of electro-optic activity – the dominating THz signal generation mechanism of the reference sample. As the second-order NLO activity is reduced for increasing annealing temperatures a current surge of free-charge carriers generated by two photon absorption will gain importance as alternative THz generation mechanism which is causing a transformation in shapes of the signal generated.

Figure 3(b) shows the corresponding terahertz amplitude gain factor defined as $\eta = \sum_{50GHz}^{1THz} \left| FFT\{E_{sample}(t)\} \right| \Big/ \sum_{50GHz}^{1THz} \left| FFT\{E_{reference}(t)\} \right|$ in dependence to the applied annealing temperatures. For the PA sample only exposed to room temperature the THz amplitude gain factor is 64. With increasing temperature the amplitude drops continuously. At 700 °C the THz amplitude gain is close to one which means that the PA induced nonlinearity has almost completely vanished. At intermediate temperatures the thermal desorption process is showing two critical temperatures where step-wise degradations occur. The region up to 150 °C is thermally stable. A significant decrease of the THz amplitude to averaged 54% is located between 150 °C and 200 °C. Then another stable region follows between 200 °C and 350 °C. Above 400 °C again the THz amplitude abruptly decreases to approx. 15% of the room temperature level.

The bond stability of $SiBr_x$ (x = 1,2,3) molecules to the silicon lattice is reduced with increasing number of Br bond atoms. Surface concentration and phases are known factors influencing the absolute desorption temperature of the corresponding $SiBr_x$ molecules [18].

#203363 - $15.00 USD Received 18 Dec 2013; revised 13 Feb 2014; accepted 17 Feb 2014; published 27 Feb 2014

From the number of degradation steps in our data one can deduce that the $SiBr_3$ and $SiBr_2$ bonds are mainly responsible for the generation of optical nonlinearity on our samples. Especially the $SiBr_2$ 3x1 surface reconstruction is known to be highly strained [22] and is therefore expected to contribute strongly to the effective nonlinearity.

Based on this thermal stability information a fabrication process for a first Mach-Zehnder modulator has been developed. To find a highly insulating cladding layer which can be processed without exceeding the first degradation step in the temperature range between 150 and 200 °C turned out to be very challenging. An acceptable compromise was found in the spin-on polymer bis-benzocyclobutene (BCB) with a curing temperature of 200 °C.

4. Electro-optic characterization

In order to put the efficiency of the PA-process into relation with other techniques, i.e. global or local strain, an electro-optic characterization of a series of devices has been applied for the quantitative determination of the underlying effective $\chi^{(2)}$ values as will be discussed in the following.

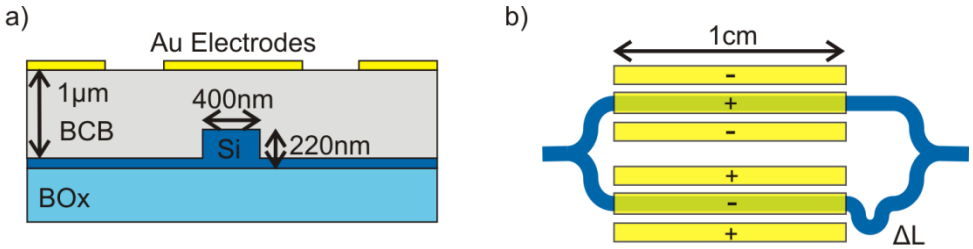

Fig. 4. Schematic of the Mach-Zehnder Device: (a) Cross section of the waveguide with electrodes on top. (b) Top view of the device with push-pull electrode configuration and a given arm asymmetry of ΔL.

The electro-optic measurements are performed in a similar fashion as published for the characterization of strained waveguides by Chmielak et al. [11]. Fully integrated Mach-Zehnder interferometer (MZI) devices, as shown in the schematic cross-section and top-view in Figs. 4(a) and 4(b), respectively, are fabricated with a waveguide width of 400 nm and a height of 220 nm. The length of each interferometer arm is approx. 1 cm. The silicon waveguide layer is covered by a 1-µm-thick spin-coated cladding layer of thermally cured BCB. On top, planar Au electrodes are structured by using a photo-lithography, a metal deposition and finally a lift-off process.

The MZIs investigated are characterized with TM-polarized light in a spectral range from 1540 nm to 1630 nm. In TM-mode the optical field distribution of the single-mode waveguide generates maximum field intensity close to the top PA-surface of the waveguide, where the highest nonlinear activity is expected. Additionally, the probed $\chi^{(2)}$ tensor component in the case of both, optical and bias fields being oriented vertically to the waveguide surface is the $\chi_{zzz}^{(2)}$ component, exhibiting the highest value of available tensor components in silicon [23].

Three transmission spectra at different bias-states measured at an exemplary MZI are shown in Fig. 5(a). The specified average field strength at the silicon waveguides in dependence on bias voltage is calculated using the numerical field solver software EM-Studio from CST. The measured transfer functions exhibit three transmission maxima of constructive interference within the monitored spectral range. The black curve is obtained at zero bias voltage. By applying a positive (red curve) or negative (green curve) voltage to the device the transfer function is blue or red shifted from the unbiased case, respectively. For the quantification of $\chi^{(2)}$, the maximum bias field was reduced to +/–11 kV/cm in order to avoid influence of any potential higher-order optical effects. The exact spectral position of a constructive interference maximum is obtained by numerical approximation of the transfer function and plotted against the applied electric field for an exemplary device in Fig. 5(b).

#203363 - $15.00 USD Received 18 Dec 2013; revised 13 Feb 2014; accepted 17 Feb 2014; published 27 Feb 2014

Hysteresis analysis of the electro-optic response is indicated by the blue/red colored points while the measurement direction is indicated by the colored arrows. Within the limits of measurement accuracy no hysteresis effects are observable. Charging of the insulator or other leakage currents can therefore be excluded as parasitic modulation effects. The linear approximation of the data points in Fig. 5(b) (as represented by the black line) exhibits that the field-induced shift of spectral interference positions is following a strictly linear function along the full modulation range. The observed behavior conclusively proves the linear Pockels-effect as the responsible modulation effect and shows that the process of plasma activation can be effectively utilized for the fabrication of silicon nanophotonic electro-optic modulator devices. Further carrier-based contributions to the observed modulation behavior (as for example a field effect induced carrier density modulation) are negligible: A reference modulator device fabricated without plasma-activation did not show any measurable spectral shift. Additionally, a linear symmetric behavior as shown by the plasma-activated modulator in this work is not expected for a carrier-based modulation.

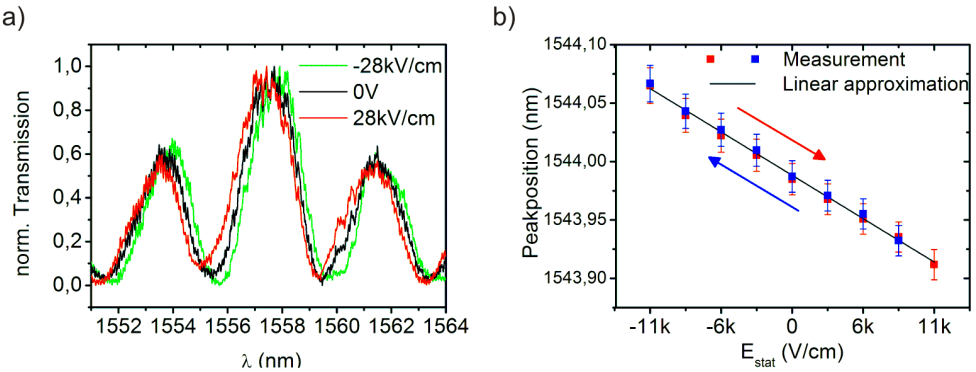

Fig. 5. Experimental electro-optic characteristic of an exemplary plasma-activated MZI. (a) Transfer function at different electrical bias fields. (b) Field-modulation of a constructive maximum position including hysteresis measurement (sweep direction as indicated by arrows).

The effective $\chi^{(2)}$ can now be quantified from the measured dependence of the spectral shift to the applied electric field under consideration of the waveguide confinement factor [24]. The confinement factor is calculated by modal simulation of the waveguide using Ansoft HFSS. From the measurement of 8 devices an average effective $\chi^{(2)}$ of the silicon waveguide of $\chi^{(2)} = 9 \pm 1$ pm/V is obtained. It has been verified by THz DFG measurements that the BCB cladding process is causing a $\chi^{(2)}$ degradation of 46%. Using curing temperatures below 150 °C an effective $\chi^{(2)}$ of 17 pm/V should be feasible.

It is worth to mention that the $\chi^{(2)}$ value determined here from dc field induction may be different from the absolute value for the THz generation case due to the dispersion relation of the second-order nonlinearity. However, both values can be expected to be very similar under the legitimate assumption of absence of electronic resonances in the considered frequency regime.

5. Discussion

The obtained value of $\chi^{(2)} = 9 \pm 1$ pm/V for the PA silicon waveguides is of comparable magnitude to the early results achieved by Jacobsen et al. [3] using global mechanical strain with a value of $\chi^{(2)} \approx 15$ pm/V. In 2012 Cazzanelli et al. demonstrated an improved $\chi^{(2)}$ of 40 ± 30 pm/V caused by strain [10]. Chmielak et al. recently showed [11,12] that locally strained nanophotonic silicon waveguides can reach even higher effective nonlinearities around 190 pm/V. However for such high effective nonlinearities very small waveguide dimensions – with widths well below 500 nm – are mandatory [12,25], which is also requiring compromises in terms of attenuation loss. In contrast, the plasma activation process

#203363 - $15.00 USD Received 18 Dec 2013; revised 13 Feb 2014; accepted 17 Feb 2014; published 27 Feb 2014

presented in this work does not require a spatial limitation of the waveguide cross-section, it rather benefits from an increased waveguide (top-)surface. Furthermore, an unprecedented flexibility for device integration is given by the simple photo-lithographic masking process which is sufficient for the fabrication of arbitrarily shaped and located chip areas of electro-optic activity. Carefully estimating the depth of influence of the chemical surface treatment to be in an order of 10 nm implies that the local maximum $\chi^{(2)}$ value within the top layer should be in the order of 190 pm/V. By using optimized (e.g. slotted) waveguide designs it should be possible to bring the currently available effective $\chi^{(2)}$ closer to this surface-near peak value, as it has been proposed in [26] for optical fibers with a surface nonlinearity. Furthermore, the spatial overlap of applied electric modulation field with the optical mode and the area of nonlinear optical activity could be strongly improved by electrode structure modification similar to polymer-based modulators presented earlier [8]. In order to take advantage of such structural modifications a plasma-activation of the waveguide sidewalls would be preferable. An adaption of the plasma-activation process will be required for this step. Also the thermal stability of the activated silicon structures might be improved by an optimization of the $SiBr_3/SiBr_2$ ratio and surface concentration. This may help to overcome the strong thermal post processing limitation of 150°C and increase the stability of the activated surface up to 400°C. The intrinsic advantages of highest modulation speeds, linear response and low linear losses may outpace carrier-based integration concepts [4] if the effective $\chi^{(2)}$ values can be further increased towards $LiNbO_3$ with $\chi^{(2)} = 360$ pm/V.

6. Conclusion

In this work we have investigated and quantified the efficiency of the HBr plasma-activation process for the induction of second-order optical nonlinearity in silicon nanophotonic structures. A fully integrated electro-optic Mach-Zehnder interferometer has been fabricated revealing an effective $\chi^{(2)}$ value of 9 ± 1 pm/V. Limiting the post-plasma-activation processing temperature below 150 °C should enable $\chi^{(2)}$ values of 17 pm/V for the discussed waveguide profiles.

The capability of simple lithographic definition of micron-scale nonlinear active areas within a single device has been experimentally demonstrated using local Terahertz difference frequency generation and constitutes an important advantage over other known methods as the application of mechanical strain or poled polymer layers. The fabrication method should pave the way for the realization of quasi-phase matched devices based on periodically activated silicon waveguides. Therefore this process has significant impact on the further development of integrated nonlinear optical components featuring CMOS-process compatibility.

Acknowledgments

This work was supported by the Deutsche Forschungsgemeinschaft (DFG) in frame of the "THz nanophotonics" project (Contract Nos. NA762/2-2 and KU540/50-2).

#203363 - $15.00 USD Received 18 Dec 2013; revised 13 Feb 2014; accepted 17 Feb 2014; published 27 Feb 2014